

Proposed new approach to the design of universal logic gates using the electro-optic effect in Mach–Zehnder interferometers

SANTOSH KUMAR,^{1,*} GURDEEP SINGH,¹ ASHISH BISHT,¹ SANDEEP SHARMA,¹ AND ANGELA AMPHAWAN^{2,3}

¹Photonics Lab, Department of Electronics & Communication Engineering, DIT University, Dehradun 248009, Uttarakhand, India

²Massachusetts Institute of Technology, Cambridge, Massachusetts 02139, USA

³InterNetWorks Research Laboratory, School of Computing, Universiti Utara Malaysia, 06010 Sintok, Kedah, Malaysia

*Corresponding author: santoshrus@yahoo.com

Received 22 June 2015; revised 28 August 2015; accepted 28 August 2015; posted 31 August 2015 (Doc. ID 243235); published 30 September 2015

Efficient application of the electro-optic effect in a lithium-niobate-based Mach–Zehnder interferometer to construct universal gates has been demonstrated. The study is carried out by simulating the proposed device with the beam propagation method, and the results are verified using MATLAB. Various parameters influencing the performance of the device (such as speed, latency, and power consumption) also have been taken into account. © 2015 Optical Society of America

OCIS codes: (230.2090) Electro-optical devices; (230.7400) Waveguides, slab; (230.3750) Optical logic devices; (250.3140) Integrated optoelectronic circuits.

<http://dx.doi.org/10.1364/AO.54.008479>

1. INTRODUCTION

Optical digital signal processing has attracted intensive research interest in recent years due to its distinctive features of high bandwidth, low distortion in signal distributions, high spectral and spatial coherence, robustness to cosmic radiations, and free RF interference. Although in the past various authors have shown their keen interest in implementing a number of digital logic gates (such as XOR, AND, and NOT) using distinct optical processing techniques [1–6], designing universal gates still remains a key issue in optical signal processing. The importance of universal logic gates (NAND and NOR) cannot be neglected. These gates are called universal because all other logic operations can be implemented with the help of these logic gates. Keeping this point in view, the usefulness in accomplishing the all-optical NOR and NAND gates using a quantum dot semiconductor optical amplifier-based Mach–Zehnder interferometer (MZI) is raised [7–9]. In this paper, a novel approach to implement universal gates using the electro-optic effect in MZI is proposed. The basic switching aspect in LiNbO₃-based MZI, owing to the electro-optic (EO) effect, is explained [10]. The LiNbO₃-based MZI is characterized by the attractive features of compact size, thermal stability [11], reconfigurability [12], integration potential [11], low latency, and low power consumption [13,14]. Many researchers have thus shown keen interest and designed various combinational

and sequential circuits using MZIs [15–23]. Implementation of universal logic gates using the electro-optic effect of LiNbO₃-based MZI has been demonstrated [24], in which authors have designed a NAND gate by inverting the output of an AND gate [25]. The authors placed a photodetector at the output, giving that output electrical signal to the second electrode of another MZI, which acts as an inverter, and the second output of this MZI gives us logical NAND operation. In a similar manner, the NOR gate [24] is designed by inverting the output of OR operation. Here, designing these universal gates using AND and OR operation does not justify the term “universal” given to them. In addition to that, six MZIs have been used in the implementation of a NOR gate, which raises concern about issues such as complexity, latency, and power consumption. For a general classical description of MZIs, readers should refer to [26] (a description using Dirac’s quantum notation is also available in the literature [27]).

This paper outlines the design process of universal gates based on the electro-optic effect of MZI. The proposed structures are implemented with the help of the beam propagation method (BPM); the results are verified with the help of MATLAB. The basic working principle, mathematical formulation, and MATLAB simulation results are presented in Section 2. The results obtained through BPM and their discussion are well presented in Section 3. Section 4 includes detailed

analysis of factors affecting the performance of the devices, and Section 5 comprises the conclusion.

2. IMPLEMENTATION OF UNIVERSAL GATES USING THE MZIS

The MZIs can be used to perform optical switching based on the principle of the EO effect. The channel waveguide can be created on the lithium-niobate substrate, as shown in Fig. 1(a). As we can see, this device contains two input ports and two output ports associated with electrodes [18]. Hence, the refractive index of one of the arms of the MZI can be changed depending upon the voltage applied across one of the arms. The optical signal can be launched to the input port; meanwhile, the light signal can be divided equally into two parts. Then, this equally divided signal propagates through the two arms, and again the signal combines, and finally, by a series of combination and distribution of signals, eventually, the output is observed at the two ports. Now, by putting the electrodes around the arms of the MZI, a kind of phase modulator can be created. The BPM simulation results for the MZI are shown in Figs. 1(b) and 1(c). By applying the 0.00 V at the second electrode of the MZI, the light signal switches to output port 2 [as shown in Fig. 1(b)], and by applying the 6.75 V at the second electrode of MZI, the light signal switches to output port 1 [as shown in Fig. 1(c)].

A. Implementation of NOR Gate

The applications of universal logic gates are essential in order to improve the flexibility in complex digital circuits. Figure 2 shows a schematic diagram of the NOR gate using MZIs. An optical signal is given to the first input port of MZI1. The first output of MZI1 is taken directly outside, and the second output port of MZI1 is connected to the second input port of MZI2. There are two outputs of MZI2. Here, the first output

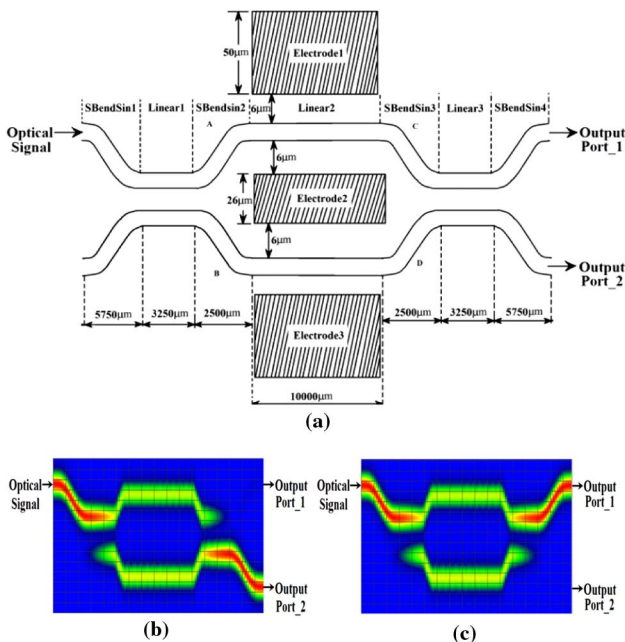


Fig. 1. (a) Diagram of MZI. (b) Switching of light signal at 0.00 V. (c) Switching of light signal at 6.75 V.

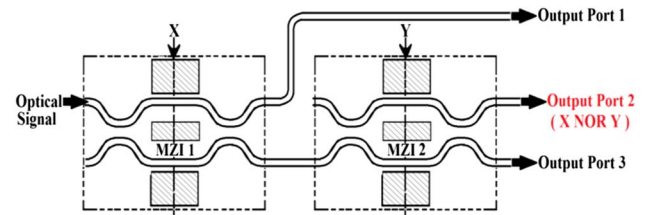


Fig. 2. Diagram of the NOR gate using the MZIs.

port of MZI2 is output port 2, which acts as the output of the NOR gate.

B. Mathematical Formulation of Normalized Power at Various Output Ports

To perform NOR operation, the normalized power at the first output port of MZI2 (Port 2 in Fig. 2) is calculated as follows.

Using the relation for single stage MZI structure [10],

$$\text{OUT}_{1\text{MZI2}} = \left\{ j e^{-j(\varphi_{0\text{MZI1}})} \cos\left(\frac{\Delta\varphi_{\text{MZI1}}}{2}\right) \right\} \times \left\{ j e^{-j(\varphi_{0\text{MZI2}})} \cos\left(\frac{\Delta\varphi_{\text{MZI2}}}{2}\right) \right\} E_{\text{in}}, \quad (1)$$

$$\frac{\text{OUT}_{1\text{MZI2}}}{E_{\text{in}}} = \left\{ j e^{-j(\varphi_{0\text{MZI1}})} \cos\left(\frac{\Delta\varphi_{\text{MZI1}}}{2}\right) \right\} \times \left\{ j e^{-j(\varphi_{0\text{MZI2}})} \cos\left(\frac{\Delta\varphi_{\text{MZI2}}}{2}\right) \right\}, \quad (2)$$

$$m_0 = \left| \frac{\text{OUT}_{1\text{MZI2}}}{E_{\text{in}}} \right|^2 = \cos^2\left(\frac{\Delta\varphi_{\text{MZI1}}}{2}\right) \cos^2\left(\frac{\Delta\varphi_{\text{MZI2}}}{2}\right). \quad (3)$$

For the calculation of Eq. (3), it has been assumed that

$$\left. \begin{aligned} \varphi_{0\text{MZI1}} &= \frac{\varphi_{1\text{MZI1}} + \varphi_{2\text{MZI1}}}{2} & \Delta\varphi_{\text{MZI1}} &= \varphi_{1\text{MZI1}} - \varphi_{2\text{MZI1}} = \frac{\pi}{V} X \\ \varphi_{0\text{MZI2}} &= \frac{\varphi_{1\text{MZI2}} + \varphi_{2\text{MZI2}}}{2} & \Delta\varphi_{\text{MZI2}} &= \varphi_{1\text{MZI2}} - \varphi_{2\text{MZI2}} = \frac{\pi}{V} Y \end{aligned} \right\} \quad (4)$$

$\varphi_{1\text{MZI1}}$ and $\varphi_{1\text{MZI2}}$ are the phase angles generated at the upper arm of MZI1 and MZI2, respectively. $\varphi_{2\text{MZI1}}$ and $\varphi_{2\text{MZI2}}$ are the phase angles generated at the lower arm of MZI1 and MZI2, respectively. MZI1 is controlled by signal X (the voltage applied at the second electrode, keeping the other two electrodes at the ground potential). Similarly, MZI2 is controlled by control signal Y. Basically, the control signals are 0 (0.00 V) and 1 (6.75 V) at the second electrodes of each MZI. Hence,

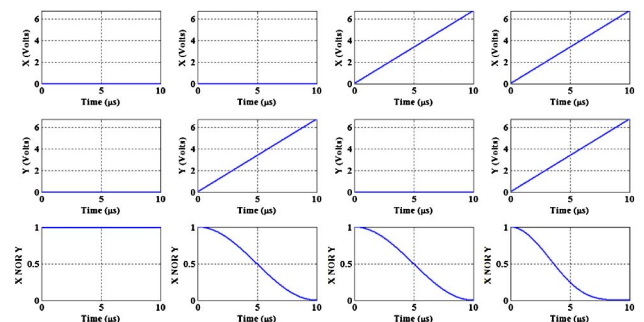


Fig. 3. MATLAB simulation result of the NOR gate.

the normalized output power at the first output port of MZI2 (output port 2 in Fig. 2) can be represented by Eq. (3). The proper combination of min-terms provides the expression of the NOR logic for the proposed NOR gate circuit. Hence, the expression for the NOR gate can be obtained by the following equation:

$$\begin{aligned} \text{Output port 2 (NOR logic gate)} &= \left| \frac{\text{OUT}_{1\text{MZI2}}}{E_{\text{in}}} \right|^2 \\ &= \cos^2\left(\frac{\Delta\varphi_{\text{MZI1}}}{2}\right) \cos^2\left(\frac{\Delta\varphi_{\text{MZI2}}}{2}\right). \end{aligned} \quad (5)$$

Figure 3 shows the simulation results of the NOR gates, where row 1 represents the control signal (X) at the second electrode of first MZI. The second row shows the control signal (Y) at the second electrode of the second MZI. Output of the NOR gate can be obtained at output port 2; the results are shown in the third row of Fig. 3. It is apparent from Fig. 3 that output is high when both inputs are low logic and outputs are low if one or both inputs are high.

C. Implementation of NAND Gate

Three MZIs are required to implement the NAND gate, as shown in Fig. 4. The optical signal is provided to the first input port of MZI1. The first output port of MZI1 is directly taken as the first output, and the second output port of MZI1 is connected to the first input port of MZI3. Again, the second optical signal is provided to the first input port of MZI2, and the second output port of MZI2 is connected to the second input port of MZI3. Here, output port 2 is acting as the NAND logic gate. Figure 5 shows the simulation result of the NAND gate,

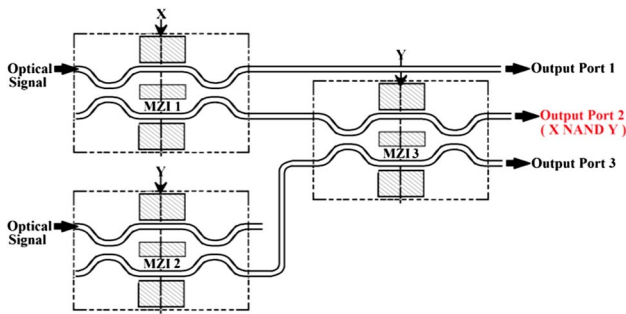


Fig. 4. Diagram of the NAND gate using the MZIs.

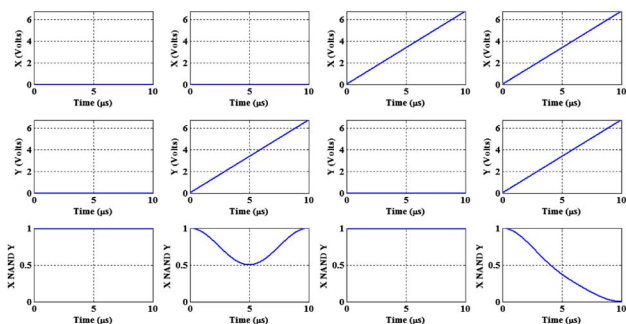


Fig. 5. MATLAB simulation result of the NAND gate.

where the first row shows the control signal (X) at the second electrode of MZI1. The second row represents the control signal (Y) at the second electrode of MZI2 and MZI3. Output of the NAND gate can be obtained at output port 2; the results are shown in the third row of Fig. 5.

D. Mathematical Formulation of Normalized Power at Various Output Ports

For all possible min-terms at the first output port of MZI3 (Port 2 in Fig. 4) (to perform a NAND operation), the normalized power is calculated as follows.

Using the relation for a single-stage MZI structure [10], the normalized output power at different output ports can be represented by Eqs. (6)–(8):

$$\begin{aligned} m_0 &= \left| \frac{\text{OUT}_{1\text{MZI3}_1}}{E_{\text{in}}} \right|^2 = \cos^2\left(\frac{\Delta\varphi_{\text{MZI1}}}{2}\right) \\ &\quad \times \cos^2\left(\frac{\Delta\varphi_{\text{MZI2}}}{2}\right) \cos^2\left(\frac{\Delta\varphi_{\text{MZI3}}}{2}\right), \end{aligned} \quad (6)$$

$$\begin{aligned} m_1 &= \left| \frac{\text{OUT}_{1\text{MZI3}_2}}{2} \right|^2 \\ &= \cos^2\left(\frac{\Delta\varphi_{\text{MZI1}}}{2}\right) \sin^2\left(\frac{\Delta\varphi_{\text{MZI2}}}{2}\right) \sin^2\left(\frac{\Delta\varphi_{\text{MZI3}}}{2}\right), \end{aligned} \quad (7)$$

$$\begin{aligned} m_2 &= \left| \frac{\text{OUT}_{\text{MZI3}_3}}{2} \right|^2 \\ &= \sin^2\left(\frac{\Delta\varphi_{\text{MZI1}}}{2}\right) \cos^2\left(\frac{\Delta\varphi_{\text{MZI2}}}{2}\right) \cos^2\left(\frac{\Delta\varphi_{\text{MZI3}}}{2}\right). \end{aligned} \quad (8)$$

For calculation of Eqs. (6)–(8), it has been assumed that

$$\left. \begin{aligned} \varphi_{0\text{MZI1}} &= \frac{\varphi_{1\text{MZI1}} + \varphi_{2\text{MZI1}}}{2} \quad \Delta\varphi_{\text{MZI1}} = \varphi_{1\text{MZI1}} - \varphi_{2\text{MZI1}} = \frac{\pi}{V_\pi} X \\ \varphi_{0\text{MZI2}} &= \frac{\varphi_{1\text{MZI2}} + \varphi_{2\text{MZI2}}}{2} \quad \Delta\varphi_{\text{MZI2}} = \varphi_{1\text{MZI2}} - \varphi_{2\text{MZI2}} = \frac{\pi}{V_\pi} Y \\ \varphi_{0\text{MZI3}} &= \frac{\varphi_{1\text{MZI3}} + \varphi_{2\text{MZI3}}}{2} \quad \Delta\varphi_{\text{MZI3}} = \varphi_{1\text{MZI3}} - \varphi_{2\text{MZI3}} = \frac{\pi}{V_\pi} Y \end{aligned} \right\} \quad (9)$$

$\varphi_{1\text{MZI1}}$, $\varphi_{1\text{MZI2}}$, and $\varphi_{1\text{MZI3}}$ are the phase angle generated at the upper arm of MZI1, MZI2, and MZI3, respectively. $\varphi_{2\text{MZI1}}$, $\varphi_{2\text{MZI2}}$, and $\varphi_{2\text{MZI3}}$ are the phase angle generated at the lower arm of MZI1, MZI2, and MZI3, respectively. MZI1 is controlled by signal X (the voltage applied at the second electrode, keeping the other two electrodes at the ground potential). Similarly, MZI2 and MZI3 are controlled by control signal Y. Basically, the control signals are 0 (0.00 V) and 1 (6.75 V) at the second electrodes of each MZI. The proper combination of min-terms provides the expression of the NAND logic for the proposed NAND gate circuit. Hence, the expression for the NAND gate can be obtained as

$$\begin{aligned}
 \text{Output port 2 (NAND Logic Gate)} &= \left| \frac{\text{OUT}_{1\text{MZI3}}}{E_{\text{in}}} \right|^2 \\
 &= m_0 + m_1 + m_2 \\
 &= \cos^2\left(\frac{\Delta\varphi_{\text{MZI1}}}{2}\right) \cos^2\left(\frac{\Delta\varphi_{\text{MZI2}}}{2}\right) \cos^2\left(\frac{\Delta\varphi_{\text{MZI3}}}{2}\right) \\
 &\quad + \cos^2\left(\frac{\Delta\varphi_{\text{MZI1}}}{2}\right) \sin^2\left(\frac{\Delta\varphi_{\text{MZI2}}}{2}\right) \sin^2\left(\frac{\Delta\varphi_{\text{MZI3}}}{2}\right) \\
 &\quad + \sin^2\left(\frac{\Delta\varphi_{\text{MZI1}}}{2}\right) \cos^2\left(\frac{\Delta\varphi_{\text{MZI2}}}{2}\right) \cos^2\left(\frac{\Delta\varphi_{\text{MZI3}}}{2}\right).
 \end{aligned} \tag{10}$$

3. IMPLEMENTATION OF UNIVERSAL GATES USING BPM

OptiBPM [14–21] is further used to analyze the proposed structure. OptiBPM is based on the finite difference beam propagation method. BPM allows computer-simulated observation of the light-field distribution. The radiation and the guided field can be examined simultaneously. The laser beam required for the operation of the proposed logic gates should operate at $1.33 \mu\text{m}$ having a linewidth of less than or equal to 100 kHz and a linewidth-power product of approximately 100 kHz-mW.

A. Implementation of the NOR Gate

Layout of the NOR gate consists of two MZIs, as shown in Fig. 6.

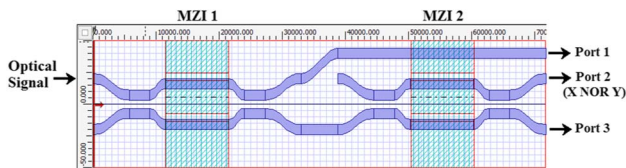


Fig. 6. Layout diagram of the NOR gate using Mach-Zehnder interferometers.

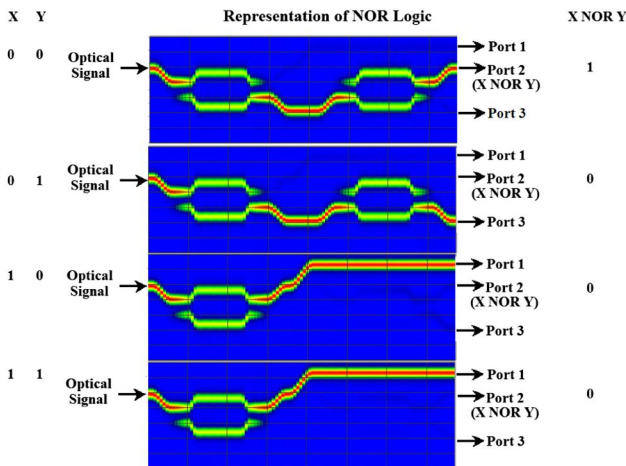


Fig. 7. Results of the NOR logic operation of the different combinations of the control signals (X and Y) obtained through the beam propagation method.

Table 1. Optical Signal at Different Ports Due to Different Combinations of Control Signals

Control Signals		Signal Output at Different Ports		
X	Y	Port 1	Port 2 (X NOR Y)	Port 3
0	0	0	1	0
0	1	0	0	1
1	0	1	0	0
1	1	1	0	0

Proper selection of control signal provides the suitable result of NOR logic, which is shown in Fig. 7. Figure 7 represents the different combinations of the control signals (electrode voltages) and their corresponding outputs at port 2. The results obtained from the proposed structure can be verified with the truth table in Table 1. MATLAB simulation results shown in Fig. 3 are exactly matched with BPM results, as shown in Fig. 7.

B. Implementation of the NAND Gate

The layout diagram of the NAND gate is shown in Fig. 8. Here, the control signals are arranged similar to the previous case.

The result of NAND logic obtained from the BPM is shown in Fig. 9. It can be verified by Table 2, which is the truth table of the NAND gate. These results also are verified with MATLAB simulation results, as shown in Fig. 5.

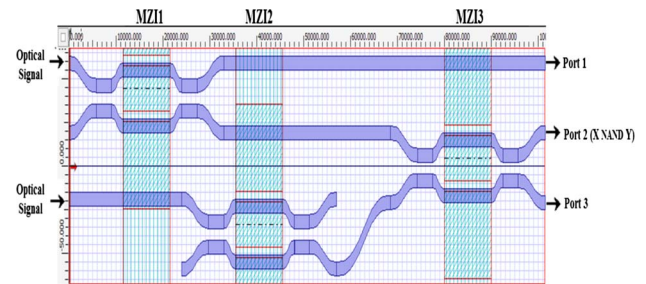


Fig. 8. Layout diagram of the NAND gate using Mach-Zehnder interferometers.

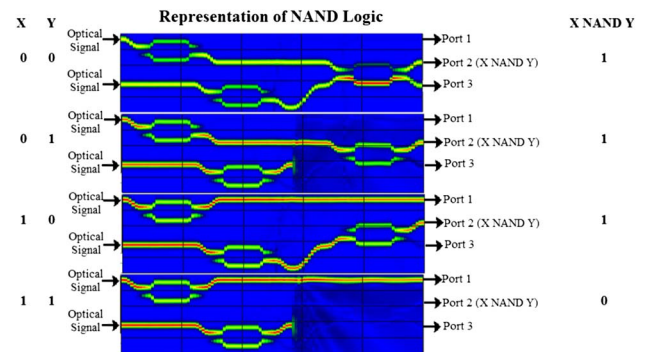


Fig. 9. Result of the NAND gate logic operation of the different combinations of the control signals (X and Y) obtained through the beam propagation method.

Table 2. Optical Signal of NAND Gate at Different Ports Due to Different Combinations of Control Signals

Control Signals		Signal Output at Different Ports		
X	Y	Port 1	Port 2 (X NAND Y)	Port 3
0	0	0	1	1
0	1	0	1	0
1	0	1	1	0
1	1	1	0	0

4. STUDY AND ANALYSIS OF SOME FACTORS INFLUENCING THE PERFORMANCE OF PROPOSED DEVICES

The performance of a single MZI, which is being used as a basic building block in the architecture of proposed devices, is examined by accomplishing the 2D-isotropic simulation using the paraxial BPM with a finite difference engine scheme parameter of 0.5 and transparent boundary condition. The global data is taken as refractive index MODAL, and TM polarized test signals with a wavelength of 1.33 μm are taken into consideration. The modal dispersion, D_m , for a multimode step-index electro-optic device with length L_m is given by [14]

$$D_m = \frac{L_m n_e \Delta n_e}{c}, \tag{11}$$

where n_e is the effective refractive index of the material (LiNbO₃) in MZI, Δn_e is the relative refractive index difference, and L_m is the length of a single MZI. Similarly, the chromatic dispersion, D_c , of a single LiNbO₃-based MZI is given by

$$D_c = -\left(\frac{L_m \Delta \lambda_0 \lambda_0}{c}\right) \cdot \left(\frac{d^2 n_e}{d\lambda^2}\right), \tag{12}$$

where λ_0 is the operating wavelength and $\Delta \lambda_0$ is the spectral linewidth of optical source. The total dispersion coefficient D_t is given by

$$D_t = D_m + D_c. \tag{13}$$

Rise time of the system in terms of bit rate (BR) for nonreturn-to-zero pulse is given by

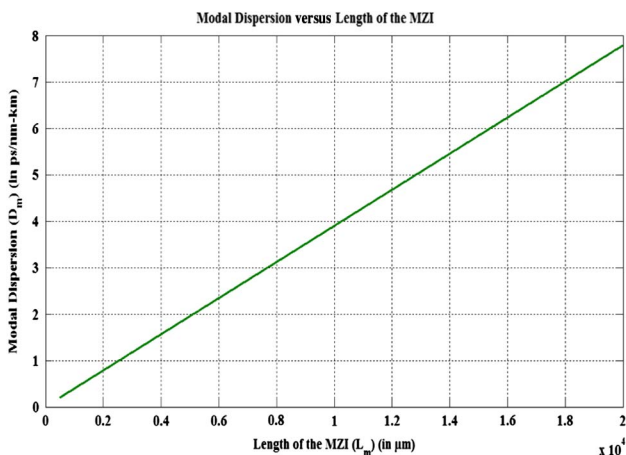


Fig. 10. Variation of modal dispersion with length of MZI.

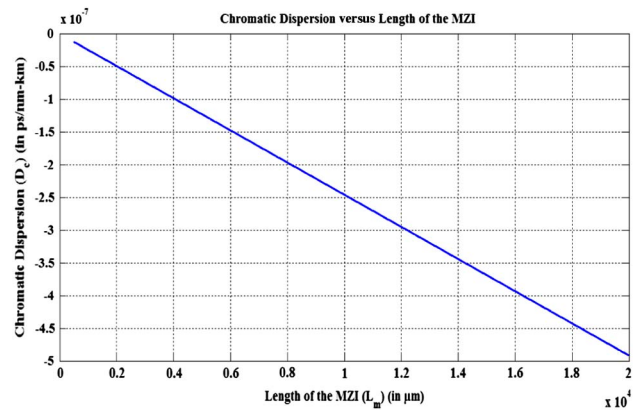


Fig. 11. Variation of chromatic dispersion with respect to length of MZI.

$$BR = \frac{0.7}{D_t}. \tag{14}$$

Figure 10 demonstrates the change of modal dispersion (D_m) in a single MZI at an operating wavelength of 1.3 μm, as the length of MZI is changed from 500 to 20,000 μm. It is apparent from the plot that, as the length of MZI is increased, D_m increases with a positive slope. In a similar manner, chromatic dispersion (D_c) carries on accumulating in the negative direction, as is apparent in Fig. 11.

Although, at smaller length, dispersion is less and pulse broadening is less. But there is a limitation in reducing the length of MZI to very small values for a specified wavelength because, as the length of MZI reduces, switching voltage required for the operation of MZI increases, as given by [10]

$$V = \frac{\lambda_0 \Delta \varphi}{n^3} \frac{1}{\pi} \frac{1}{r L}, \tag{15}$$

where λ_0 is the wavelength of light used, $\Delta \varphi$ is the phase change owing to the applied electric field, r is electro-optic coefficient ($\cong 36.6 \times 10^{-12}$ m/V for LiNbO₃), and d is the separation between electrodes, and it cannot be reduced below a certain optimized value. If we try to decrease the separation below a certain value, the electric field might become larger than the

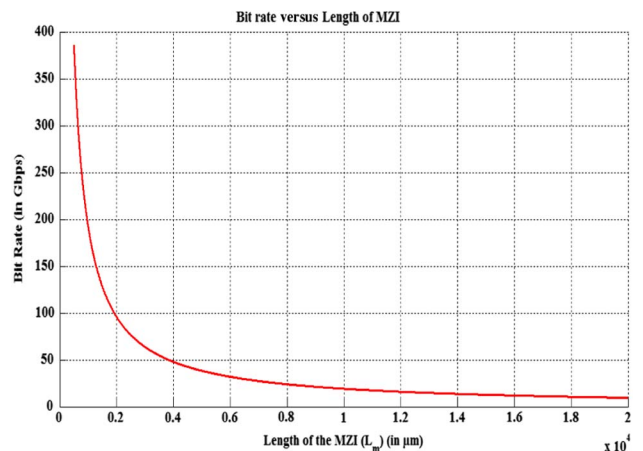


Fig. 12. Variation of bit rate with respect to length of MZI.

breakdown field. L is the substantial length. Also, the available length is not sufficient to couple energy from one waveguide to other.

But still, by optimizing various parameters such as length of MZI, switching voltage, and wavelength of operation, a bit rate of the order of 20–200 Gbps can be obtained, as shown in Fig. 12. Thus, by selecting the appropriate length of MZI, low power consumption structure with low latency and high speed can be obtained.

The transition losses for straight and curved waveguides with the variation of Ti-diffusion thickness in the range of 0.04–0.09 μm can be observed [16].

5. CONCLUSION

This paper includes detailed discussion on the design of universal digital logic gates (NOR and NAND gates) using the electro-optic effect in MZIs. The discussed method to implement the proposed devices is simulated using BPM; the results are verified using MATLAB. The performance analysis shows that, by optimizing various parameters such as length of MZI, switching voltage, and wavelength of operation, low-power consumption structures with low latency and high speed can be obtained.

Funding. DIT University, Dehradun, India (DITU/R&D/2014/7/ECE).

Acknowledgment. The authors would like to thank Professor K. K. Raina, vice chancellor, DIT University, Dehradun, India, for encouragement and support during the present research work.

REFERENCES

1. Y. Ishizaka, Y. Kawaguchi, K. Saitoh, and M. Koshiba, "Design of ultra compact all-optical XOR and AND logic gates with low power consumption," *Opt. Commun.* **284**, 3528–3533 (2011).
2. H. Sun, Q. Wang, H. Dong, and N. K. Dutta, "XOR performance of a quantum-dot semiconductor optical amplifier-based Mach-Zehnder interferometer," *Opt. Express* **13**, 1892–1899 (2005).
3. H. Han, M. Zhang, P. Ye, and F. Zhang, "Parameter design and performance analysis of an ultrafast all-optical XOR gate based on quantum-dot semiconductor optical amplifiers in nonlinear Mach-Zehnder interferometer," *Opt. Commun.* **281**, 5140–5145 (2008).
4. E. Dimitriadou and K. E. Zoiros, "On the design of ultrafast all-optical NOT gate using quantum-dot semiconductor optical amplifier-based Mach-Zehnder interferometer," *Opt. Laser Technol.* **44**, 600–607 (2012).
5. A. Kotb and K. E. Zoiros, "Simulation of all-optical logic XNOR gate based on quantum-dot semiconductor optical amplifiers with amplified spontaneous emission," *Opt. Quantum Electron.* **45**, 1213–1221 (2013).
6. E. Dimitriadou and K. E. Zoiros, "Proposal for ultrafast all-optical XNOR gate using single quantum-dot semiconductor optical amplifier-based Mach-Zehnder interferometer," *Opt. Laser Technol.* **45**, 79–88 (2013).
7. E. Dimitriadou and K. E. Zoiros, "On the feasibility of ultrafast all-optical NAND gate using single quantum-dot semiconductor optical amplifier-based Mach-Zehnder interferometer," *Opt. Laser Technol.* **44**, 1971–1981 (2012).
8. E. Dimitriadou and K. E. Zoiros, "Proposal for all-optical NOR gate using single quantum-dot semiconductor optical amplifier-based Mach-Zehnder interferometer," *Opt. Commun.* **285**, 1710–1716 (2012).
9. E. Dimitriadou and K. E. Zoiros, "On the design of reconfigurable ultrafast all-optical NOR and NAND gates using a single quantum-dot semiconductor optical amplifier-based Mach-Zehnder interferometer," *J. Opt.* **14**, 105401 (2012).
10. S. K. Raghuvanshi, A. Kumar, and S. Kumar, "1 \times 4 signal router using three Mach-Zehnder interferometers," *Opt. Eng.* **52**, 035002 (2013).
11. E. L. Wooten, K. M. Kissa, A. Y. Yan, E. J. Murphy, D. A. Lafaw, P. F. Hallemeier, D. Maack, D. V. Attanasio, D. J. Fritz, G. J. McBrien, and D. E. Bossi, "A review of lithium niobate modulators for fiber-optic communications systems," *IEEE J. Sel. Top. Quantum Electron.* **6**, 69–82 (2000).
12. H. Jin, F. M. Liu, P. Xu, J. L. Xia, M. L. Zhong, Y. Yuan, J. W. Zhou, Y. X. Gong, W. Wang, and S. N. Zhu, "On-chip generation and manipulation of entangled photons based on reconfigurable lithium-niobate waveguide circuits," *Phys. Rev. Lett.* **113**, 103601 (2014).
13. G. Singh, V. Janyani, and R. P. Yadav, "Modeling of a high performance Mach-Zehnder interferometer all optical switch," *Optica App.* **42**, 613–625 (2012).
14. S. Kumar, G. Singh, and A. Bisht, "4x4 signal router based on electro-optic effect of Mach-Zehnder interferometer for wavelength division multiplexing applications," *Opt. Commun.* **353**, 17–26 (2015).
15. A. Kumar, S. Kumar, and S. K. Raghuvanshi, "Implementation of XOR/XNOR and AND logic gates using Mach-Zehnder interferometers," *Optik* **125**, 5764–5767 (2014).
16. A. Kumar, S. Kumar, and S. K. Raghuvanshi, "Implementation of full-adder and full-subtractor based on electro-optic effect in Mach-Zehnder interferometer," *Opt. Commun.* **324**, 93–107 (2014).
17. S. Kumar, A. Bisht, G. Singh, K. Choudhary, and D. Sharma, "Implementation of wavelength selector based on electro-optic effect in Mach-Zehnder interferometers for high speed communications," *Opt. Commun.* **350**, 108–118 (2015).
18. S. Kumar, S. K. Raghuvanshi, and A. Kumar, "Implementation of optical switches by using Mach-Zehnder interferometer," *Opt. Eng.* **52**, 097106 (2013).
19. S. K. Raghuvanshi, A. Kumar, and N. K. Chen, "Implementation of sequential logic circuits using the Mach-Zehnder interferometer structure based on electro-optic effect," *Opt. Commun.* **333**, 193–208 (2014).
20. S. Kumar, G. Singh, A. Bisht, and A. Amphawan, "Design of D flip-flop and T flip-flop using Mach-Zehnder interferometers for high-speed communication," *Appl. Opt.* **54**, 6397–6405 (2015).
21. S. Kumar, G. Singh, A. Bisht, and A. Amphawan, "An optical synchronous up counter based on electro-optic effect of lithium niobate based Mach-Zehnder interferometers," *Opt. Quantum Electron.*, doi:10.1007/s11082-015-0234-y (to be published).
22. S. Kumar, A. Bisht, G. Singh, and A. Amphawan, "Implementation of 2-bit multiplier based on electro-optic effect in Mach-Zehnder interferometers," *Opt. Quantum Electron.*, doi:10.1007/s11082-015-0249-4 (to be published).
23. S. Kumar, S. K. Raghuvanshi, and B. M. A. Rahman, "Design of universal shift register based on electro-optic effect of LiNbO₃ in Mach-Zehnder interferometer for high speed communication," *Opt. Quantum Electron.*, doi:10.1007/s11082-015-0226-y (to be published).
24. S. K. Raghuvanshi, A. Kumar, and A. Rahman, "Implementation of high speed optical universal logic gates using the electro-optic effect-based Mach-Zehnder interferometer structures," *J. Mod. Opt.* **62**, 978–988 (2015).
25. S. Kumar, A. Kumar, and S. K. Raghuvanshi, "Implementation of an Optical AND Gate using Mach-Zehnder Interferometers," *Proc. SPIE* **9131**, 913120 (2014).
26. W. H. Steel, *Interferometry* (Cambridge University, 1967).
27. F. J. Duarte, *Quantum Optics for Engineers* (CRC Press, 2014).